BIOCHEMISTRY

 Volume 43, Number 33 August 24, 2004

Articles

Protein Dynamics and Enzymatic Catalysis: Investigating the Peptidyl−Prolyl Cis−Trans Isomerization Activity of Cyclophilin A†

Pratul K. Agarwal,* Al Geist, and Andrey Gorin

Computational Biology Institute and Computer Science and Mathematics Division, Oak Ridge National Laboratory, Oak Ridge, Tennessee 37831

Received March 10, 2004; Revised Manuscript Received June 11, 2004

ABSTRACT: A growing body of evidence suggests a connection between protein dynamics and enzymatic catalysis. In this paper, we present a variety of computational studies designed to investigate the role of protein dynamics in the detailed mechanism of peptidyl−prolyl cis−trans isomerization catalyzed by human cyclophilin A. The results identify a network of protein vibrations, extending from surface regions of the enzyme to the active site and coupled to substrate turnover. Indications are that this network may have a role in promoting catalysis. Crucial parts of this network are found to be conserved in 10 cyclophilin structures from six different species. Experimental evidence for the existence of this network comes from previous NMR relaxation studies, where motions in several residues, forming parts of this network, were detected only during substrate turnover. The high temperature factors (from X-ray crystal structures) associated with the network residues provide further evidence of these vibrations. Along with the knowledge of enzyme structure, this type of network could provide new insights into enzymatic catalysis and the effect of distant ligand binding on protein function. The procedure outlined in this paper is general and can be applied to other enzymatic systems as well. This presents an interesting opportunity; collaborative experimental and theoretical investigations designed to characterize in detail the nature and function of this type of network could enhance the understanding of protein dynamics in enzymatic catalysis.

Enzyme function depends on protein structure. A growing body of evidence from ongoing investigations continues to reveal that proteins are dynamic assemblies with a close link between structure and dynamics. Therefore, there is considerable interest in studying protein dynamics in relation with enzyme function. Understanding the role of protein dynamics in enzymatic catalysis is proving to be a challenging task (*1*, *2*). Protein dynamics[1] has been implicated in many aspects of enzyme function, including substrate−cofactor binding and release. Its connection with the substrate turnover step, however, has been difficult to ascertain (*3*). Biochemical studies have observed motions in active site and distal residues occurring along the catalytic step (*4*−*13*). These investigations have provided valuable information about protein dynamics along a section of the reaction path or at

† This research used resources of the Center for Computational Sciences at Oak Ridge National Laboratory (ORNL), which is supported by the Office of Science of the U.S. Department of Energy under Contract DE-AC05-00OR22725. This work was conducted as a part of collaborative research between IBM Corp. and ORNL, and was also supported in part by an appointment to Postdoctoral Research Associates Program administered by ORISE and ORNL.

* To whom correspondence should be addressed. E-mail: agarwalpk@ornl.gov. Phone: (865) 574-7184. Fax: (865) 576-5332.

[1] The term protein dynamics has been previously used in different contexts; here we use it to describe internal protein motions occurring at all time scales.

10.1021/bi0495228 CCC: $27.50
Published on Web 07/29/2004

a select time scale. The internal motions of proteins, however, occur over a wide range of time scales, ranging from femtosecond to second (*4*, *5*, *9*, *14*−*24*); collective information over multiple time scales is highly desirable. Together with the knowledge of protein structure, detailed information about protein dynamics at multiple time scales could provide a better understanding of enzymatic catalysis.

Theoretical and computational studies are providing information complementing the biochemical studies, thereby enhancing the understanding of protein dynamics at different time scales. Brooks and co-workers (*25*, *26*) have reported correlated motions coupled to hydride transfer in dihydrofolate reductase. Schwartz and co-workers (*27*, *28*) have identified a promoting vibration, occurring on a subpicosecond time scale, in the active site of liver alcohol dehydrogenase. Agarwal et al. (*29*, *30*) have identified and characterized a network of coupled promoting motions for hydride transfer in dihydrofolate reductase, which has been confirmed by Truhlar, Gao, and co-workers (*31*). Additional reports from other research groups have also provided valuable contributions to this area (*32*−*37*). Here we describe computational studies which have identified a network of protein vibrations that is closely coupled with the cis−trans isomerization catalyzed by human cyclophilin A (CypA).[2] The approach described here provides insights into protein dynamics at multiple time scales for CypA and can be applied to other enzymatic systems, as well.

CypA is involved in many biological reactions, including protein folding and intracellular protein transport (*38*, *39*). It is a ubiquitously expressed cytosolic protein, and is the major intracellular receptor protein for the immunosuppressive drug cyclosporin A (*40*). CypA is a peptidyl−prolyl cis−trans isomerase (PPIase) (*41*, *42*), which catalyzes the isomerization of peptidyl−prolyl amide bonds, which are N-terminal to proline residues in a wide variety of peptides and protein substrates (*38*, *43*). CypA is required for the infectious activity of HIV-1 (*44*, *45*). It is packed into the virion and most likely facilitates the disassembly of the capsid core by accelerating the cis−trans isomerization (*46*). Several mechanisms have been proposed for the prolyl isomerization reaction catalyzed by PPIases, which remain a subject of debate (*12*, *43*, *47*−*55*). In this work, we have assumed a mechanism which proceeds without formation of a tetrahedral complex or cleavage and/or formation of covalent bonds. The results of our investigations are in agreement with structural insights and a proposed reaction mechanism based on recent crystallographic studies (*54*).

Recent NMR relaxation experiments indicate that protein dynamics is linked to the PPIase activity of CypA (*10*, *12*). These experiments detected motions for the backbone of several amino acid residues (including catalytically important Arg55, and Asn102 of the active site) only during substrate turnover. On the basis of observed motions of these and other residues, an enzymatic cycle in which the motions within the protein coincide with the rate of substrate isomerization was proposed. The detailed role of many residues displaying large motions, however, is still not clear in the isomerization mechanism. These NMR experiments are a motivating factor for this study, in which we have investigated structural changes and protein dynamics at multiple time scales, coupled to the PPIase activity in CypA.

The PPIase activity of CypA has also been the subject of other recent computational studies. Bruice and co-workers performed MD simulations of the reactant, transition state (TS), and product configurations for CypA in complex with peptide substrates (*53*). Using the near-attack conformation approach, the study reported structural insights into the reaction. The roles of several active site residues (including Arg55 and Asn102) were identified. Backbone motions for Arg55 were not observed. It is important to note that parts of CypA were fixed (outside a 25 Å sphere) with positional harmonic restraints during the entire simulations reported in this study. More recently, Cui and co-workers (*55*) have reported results from their hybrid QM/MM studies aimed at investigating the role of Arg55. They found that the catalytic role of Arg55 mainly involves stabilization of the peptide substrate by strong interactions between the guanidino group and the backbone of the target proline. No effect of protein motions on catalysis on the nanosecond time scale was observed. However, authors stated that protein dynamics on the sub-millisecond time scale may play a role in catalysis.

In this paper, we describe a series of computational studies designed to investigate the role of dynamics of various protein parts in the detailed mechanism of cis−trans isomerization catalyzed by human CypA. We have calculated protein vibrations on the time scale of the isomerization reaction, investigated the dynamical flexibility of the backbone, and compared β-factors from X-ray structures, obtained dynamical correlations between protein regions, monitored conserved residues over the course of reaction, and performed structural analysis with other cyclophilin structures. The results indicate that many conserved residues in the active site and distal to the active site display a high degree of correlated motions, and constitute a part of a network of protein vibrations coupled to the reaction. These vibrations occur on time scales ranging from picosecond to microsecond−millisecond (corresponding to the time scale of reaction). Early indications are that this network may have a role in promoting catalysis. This presents an opportunity for collaborative experimental and theoretical studies, which could enhance the understanding of protein dynamics and its role in protein function. The presence of these vibrations has recently been confirmed during CypA-catalyzed cis−trans isomerization in the N-terminal domain of the capsid protein (CA^N) from HIV-1 (*56*). This capsid protein is a naturally occurring and biologically relevant substrate for CypA.

MATERIALS AND METHODS

Genomic Analysis for Sequence Conservation. The genomic analysis for sequence conservation was performed by aligning protein sequences of peptidyl−prolyl cis−trans isomerase type proteins (PPIases, EC 5.2.1.8). A total of 197 PPIase type sequences were obtained from a SwissPROT and TrEMBL database search (*57*). To avoid divergent sequences, 50 sequences that were most similar to that of human CypA were selected for alignment. These sequences

[2] Abbreviations: CA^N, N-terminal domain of capsid protein; CypA, cyclophilin A; DCCM, dynamical cross-correlation map; HIV-1, human immunodeficiency virus type 1; MD, molecular dynamics; NMR, nuclear magnetic resonance; PMF, potential of mean force; PPIase, peptidyl−prolyl cis−trans isomerase; rms, root-mean-square; TS, transition state; WHAM, weighted histogram analysis method.

belong to following species: *Escherichia coli*, *Haemophilus influenzae*, *Pseudomonas aeruginosa*, *Helicobacter pylori*, *Bacillus subtilis*, *Synechococcus* sp. (strain PCC 7942), *Synechocystis* sp. (strain PCC 6803), *Treponema pallidum*, *Streptomyces chrysomallus*, *Mycobacterium tuberculosis*, *Paramecium primaurelia*, *Candida albicans*, *Schizosaccharomyces pombe*, *Saccharomyces cerevisiae*, *Caenorhabditis elegans*, *Allium cepa*, *Brassica napus*, *Lupinus luteus*, *Catharanthus roseus*, *Arabidopsis thaliana*, *Echinococcus granulosus*, *Zea mays*, *Hemicentrotus pulcherrimus*, *Schistosoma mansoni*, *Lycopersicon esculentum*, *Drosophila melanogaster*, *Blattella germanica*, *Cricetulus longicaudatus*, *Bos taurus*, *Mus musculus*, *Rattus norvegicus*, and *Homo sapiens*. Clustal-W (*58*) was used for sequence alignment. The program default parameter values were used.

CypA−Substrate Model Preparation and Molecular Dynamics (MD) Simulations. Three equivalent simulations (termed Sim types) were carried out for CypA−substrate models based on three different X-ray structures of human CypA available from the Protein Data Bank (PDB): (1) SimAWQ, starting structure from Vajdos et al. (*59*) (PDB entry 1AWQ), with substrate His-Ala-Gly-*trans*-Pro-Ile-Ala; (2) SimCYH, starting structure from Zhao and Ke (*51*) (PDB entry 2CYH), with substrate Ala-*cis*-Pro; and (3) SimRMH, starting structure from Zhao and Ke (*50*) (PDB entry 1RMH; only monomer A was simulated), with substrate succinyl-Ala-Ala-*cis*-Pro-Phe-*p*-nitroanilide.

For each Sim type, the model included all 165 amino acids, the substrate peptide, and explicit solvent (water molecules found in the crystal structure were included). Coordinates for the missing first residue were generated on the basis of another human CypA crystal structure (PDB entry 1BCK). Structure preparation and all MD simulations were performed with the AMBER 7.0 biomolecular simulation programs and parm98 force field (*60*, *61*). Standard AMBER building blocks were used for amino acids, and new building blocks (succinic acid and 4-nitroaniline) were generated by following the procedure described in the AMBER manual. The protonation states for residues with polar side chains were identified at pH 7.0. The protonation states of the histidine residues were determined by examining the hydrogen bonding structures; all four histidines were protonated at $N_{\delta 1}$. The protonated form was used for all four cysteine residues. Other missing hydrogens were added. Each system was made charge neutral by addition of counterions; SimAWQ and SimCYH each required addition of one Cl^- ion, while SimRMH was found to be charge neutral without addition of any counterions. The structures were placed in a rectangular box of TIP3P (*62*) water, and the dimensions of the box were chosen so that the minimum distance between the solute and the side of the box was 10 Å.

The solvated complex was equilibrated using a procedure described in ref *56*. The equilibrated complex was used as the starting structure for free energy profile generation. The total number of atoms and final simulation box size for the three Sim types were as follows: (1) SimAWQ, 21 862 atoms (6598 water molecules), final simulation box size of 64.96 Å × 57.62 Å × 58.29 Å; (2) SimCYH, 22 892 atoms (6955 water molecules), final simulation box size of 63.92 Å × 59.52 Å × 60.10 Å; and (3) SimRMH, 20 865 atoms (6265 water molecules), final simulation box size of 58.93 Å × 59.30 Å × 59.57 Å.

All production phase MD runs were performed under the NVE ensemble, with the periodic boundary condition with explicit solvent, and the other conditions were the same as those in production runs in ref *56*. The time step for all MD simulations (equilibration and production) was 1.0 fs.

Models for Only Substrate Peptide in Water. For generation of free energy profiles for reaction in water (without the enzyme), substrate peptides in the water box were prepared using the procedure described above. These models (termed Pep types), PepAWQ, PepCYH, and PepRMH, correspond to CypA−substrate models SimAWQ, SimCYH, and SimRMH, respectively. The initial substrate peptide coordinates were obtained from the corresponding X-ray structure. The total number of atoms and final simulation box size for the three Pep types were as follows: (1) PepAWQ, 3962 atoms (1294 water molecules), final simulation box size of 32.33 Å × 39.01 Å × 31.68 Å; (2) PepCYH, 2010 atoms (661 water molecules), final simulation box size of 27.42 Å × 28.56 Å × 25.90 Å; and (3) PepRMH, 4536 atoms (1485 water molecules), final simulation box size of 30.30 Å × 39.93 Å × 37.95 Å.

Free Energy Profile for the Isomerization Reaction. The cis−trans isomerization of the prolyl peptide bond was simulated using a series of MD runs, in combination with the umbrella sampling technique (*63*, *64*). The free energy profile for the complete 360° rotation of the peptide bond was calculated using the weighted histogram analysis method (WHAM) (*65*). Seventy-two separate MD runs, each representing a 5° window of peptide bond rotation, were used to obtain the potential of mean force representation (PMF) for the free energy profile as a function of peptide bond rotation. WHAM has been previously used to calculate the PMF along a single coordinate (*66*, *67*) and for the cis−trans isomerization reaction (*68*).

For umbrella sampling, the amide bond dihedral angle (ω) of the peptide bond was harmonically restrained at 5° increments beginning from the equilibrated structure prepared from the starting X-ray structure. The procedure described in ref *56* was used for data generation and collection. For each window, 20 ps of MD for equilibration was followed by a production run of 400 ps. Only solute coordinates were stored after every 0.01 ps; a total of 2 880 000 structures were collected from all production MD runs (total simulation time of 28.8 ns) separately for each Sim and Pep type. During these data collection runs, the peptide bond was restrained using a harmonic force constant of 0.05 kcal mol^{-1} deg^{-2} for umbrella sampling. The final free energy profile was calculated with WHAM, using a convergence criterion of 1×10^{-4} kcal/mol.

Longer MD Trajectories for Trans, TS, and Cis States, and Averaged Structures. Extended MD simulations, for a total period of 2 ns, were carried out for the nearest ω windows corresponding to trans (reactant), TS (transition state), and cis (product) states. On the basis of free energy profiles, the trans state is located at $\omega = 180°$ and cis at $\omega = 0°$, while the TS is located at $\omega = 96.2°$, 103.3°, and 104.3° for SimAWQ, SimCYH, and SimRMH, respectively. Averaged structures were obtained by averaging 50 structures with $\omega \pm 0.5°$ of the corresponding state.

Cross-Correlation Coefficients and Dynamic Cross-Correlation Maps. Cross-correlation coefficients (*56*, *69*, *70*) were obtained on the basis of the conformations of CypA−

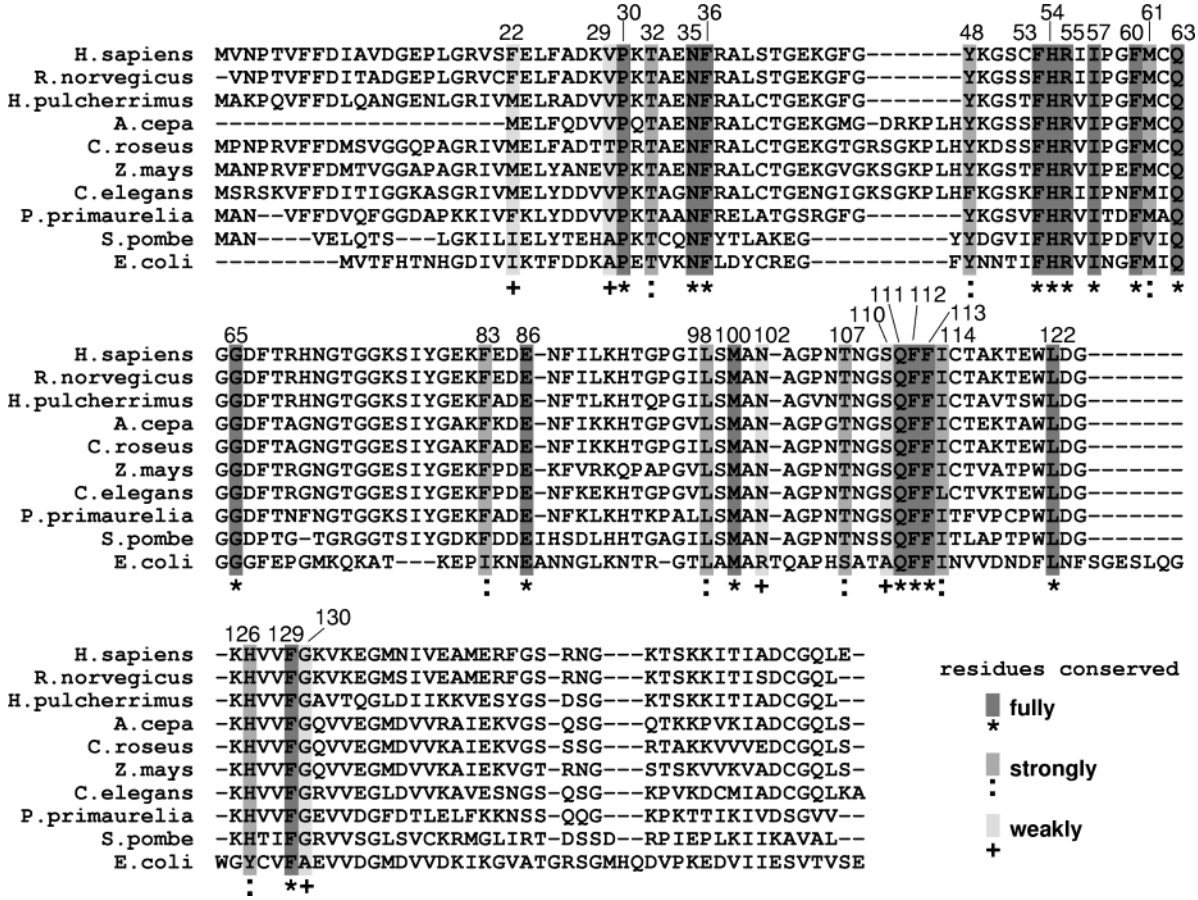

FIGURE 1: Genomic analysis for sequence conservation of CypA. Residues highlighted with a darker background are more strongly conserved. Fifty PPIase type sequences were used for analysis; only 10 representative sequences are listed here.

substrate complexes sampled during the MD simulations. The matrix of cross-correlation coefficients can be visualized as a dynamical cross-correlation map (DCCM) (*71*). Values closer to 1.0 represent regions with positive correlation, and those closer to −1.0 represent anticorrelated motions.

Forty thousand regularly spaced structures from the 2 ns of MD simulations were used for cross-correlation coefficients and DCCM calculations. Only the CypA and peptide substrate coordinates were used. Before the calculation of correlation coefficients, the structures were superimposed on a common reference structure to remove any translation and rotations introduced during the course of simulation.

Protein Vibrations. Protein vibrations in the CypA−substrate complex were identified by quasi-harmonic analysis (*56*, *72*, *73*). The atomic fluctuation matrix, required for calculation of protein vibrational modes, was constructed for only solute atoms (from CypA and substrate peptide) using a total of 18 500 structures from MD simulations in 37 windows representing the progress of the reaction from the trans form to the cis form (ω = 180°, 175°, ..., 0°). MD simulation for each window was 400 ps in duration, and 500 evenly separated (after every 0.8 ps) structures were used from each window. Before construction of the atomic fluctuation matrix, the structures were superimposed onto a common reference structure to remove any translations or rotations. Note that in our calculations, the reaction coordinate degree of freedom is effectively removed by restraints applied on the amide bond dihedral angle for the umbrella sampling. For computational reasons, only the first 50 eigenvectors were calculated.

Distance Profiles. Variation of key interactions and select distances over the course of isomerization was monitored using the conformations sampled in MD runs. For generation of the distance profiles for each Sim type, 2 880 000 collected structures were separated in histogram bins based on the value of ω. Bins 1° in width were used, ranging from −180° to 180°. The distance under consideration was calculated for all structures in each bin and averaged after the top and bottom 1% were excluded as noise. Resulting profiles were plotted for only the change in ω from the trans state to the cis state (counterclockwise rotation, 180 bins). Adjacent averaging in 10 bins was used for the final figures.

Quantum-Mechanical Modeling of the Active Site. Quantum-mechanical (electronic structure) calculations were performed on a 192-atom model of the active site (consisting of CypA residues 55, 60, 61, 102, 103, 113, 122, and 126 and residues 3−5 from the SimAWQ substrate). After the system had been displaced along protein vibrational modes, three minimization steps were performed and the energy of the last step was considered. These calculations were performed using Gaussian98 with the restricted Hartree−Fock (RHF) method, using the standard double-ζ quality 3-21G basis set (*74*).

RESULTS

Genomic Analysis for CypA Sequence Conservation. The results of multiple-sequence alignment for identification of conserved residues in CypA are summarized in Figure 1. This genomic analysis was performed by aligning 50 PPIase protein sequences from more than 25 diverse organisms.

Seventeen of 165 amino acid residues in the human CypA sequence were found to be conserved in all 50 PPIase sequences that were examined: Pro30, Asn35, Phe36, Phe53, His54, Arg55, Ile57, Phe60, Gln63, Gly65, Glu86, Met100, Gln111, Phe112, Phe113, Leu122, and Phe129. Eight additional residues were found to be strongly conserved: Thr32, Tyr48, Met61, Phe83, Leu98, Thr107, Ile114, and His126. Five other residues were found to be weakly conserved: Phe22, Val29, Asn102, Ser110, and Gly130.

Inspection of the human CypA three-dimensional structure reveals that many of these conserved residues (Arg55, Phe60, Met61, Gln63, Asn102, Phe113, Leu122, and His126) are located in the active site and interact with the substrate peptide. Several conserved residues, however, are located considerable distance from the active site. Phe83 and Glu86 are located more than 17 Å from the active site, while Pro30, Asn35, and Phe36 are located more than 18 Å away. Some of these distal residues may be conserved for structural reasons or for their role in protein folding. NMR relaxation studies, however, have indicated that the backbone of Leu98 (which is more than 12 Å from active site) exhibits motion only in the presence of substrate (*12*). Arg55, Asn102, and Ser110 also display motions in the presence of the substrate. To understand the role of these conserved residues in catalysis, their dynamics and interaction with the substrate were investigated as described below.

Free Energy Profiles. Three completely independent but equivalent simulations of the CypA−substrate complex were performed (termed Sim types) to rule out any bias from starting X-ray structure and to ensure the reproducibility of the results. These simulations differ in the starting X-ray structure, the substrate peptide, and the direction of reaction mapping (reactant → product or product → reactant). For SimAWQ (trans form in the X-ray structure), the reaction was mapped from the trans (reactant) to cis (product) conformation, while for SimCYH and SimRMH (cis form in X-ray structures), the reaction was mapped from the cis (product) to trans (reactant) conformation. No mixing of structures or states between different Sim types was performed; an independent and complete reaction profile was generated for each Sim type. These simulations, performed in opposite directions, also rule out sampling biases which may be introduced because of the direction of reaction profile generation.

Figure 2 depicts free energy profiles for the cis−trans isomerization reaction investigated in this study. The first plot corresponds to only the substrate peptide undergoing isomerization in water (without the enzyme), and the second plot depicts the free energy profiles for isomerization reaction in the presence of human CypA. These profiles indicate that the catalysis by CypA lowers the activation free energy for the counterclockwise rotation[3] by about 5 kcal/mol. The activation free energy in the presence of enzyme for counterclockwise rotation (from the trans form to the cis form) is in the range of 5−6 kcal/mol, which is ≈2 kcal/mol lower than the barrier for the corresponding clockwise rotation. These calculated values lie within a wide range of experimental values reported for different substrates catalyzed

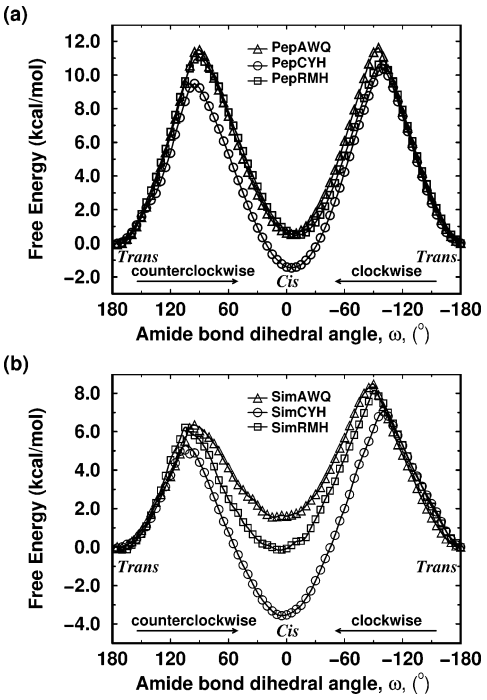

FIGURE 2: Free energy profiles for isomerization of the prolyl peptide bond (a) in water (b) catalyzed by human cyclophilin A. Results for the complete rotation of the peptide bond from three alternative simulations are presented.

by PPIases (*75*−*78*). Note that our estimates represent approximate lower bounds for the activation free energy, as in the present calculations corrections used in other enzyme studies have not been applied and a transmission coefficient[4] of 1 has been assumed (*79*, *80*). The calculations and discussions presented in the remainder of this paper pertain only to counterclockwise rotation (trans to cis) with the lower free energy of activation.

It is important to note that the collective reaction coordinate for the isomerization reaction in this study corresponds to the rotation of the peptide bond. The peptide bond was rotated (in 5° steps) to drive the reaction. Adequate sampling, using the umbrella sampling technique in 72 windows, was performed to obtain continuous sampling over the entire reaction path.

Structural Changes. Detailed analysis of the structural changes in enzyme−substrate complexes during the course of reaction was performed. Superposition of average structures from the trans (reactant), TS, and cis (product) states indicates there is little difference in the overall protein conformation. The CypA backbone shows good overlap, except in the loop regions comprised of residues 12−15, 66−74, 78−86, and 146−154.

Inspection of the active site indicates that during the course of the reaction there are minimal structural changes; most of these changes are localized toward the N-terminus of the target proline. Figure 3 shows the substrate superimposed from trans, TS, and cis states in the CypA active site. This figure indicates that the Pro*N*(S)[5] ring remains essentially fixed in the hydrophobic pocket, while the oxygen of the

[3] Based on rotation of O from the preceding residue when viewed from the proline N atom along the bond between the proline N atom and the preceding residue C atom.

[4] In enzymes, which are dynamical systems, the environment may cause the reaction trajectories to recross the dividing surface at the transition state (see refs *30* and *31*). The transmission coefficient is a corrective prefactor for these dynamical effects.

Table 1: Key Active Site Distances Calculated from Average Trans, TS, and Cis Structures (all distances in angstroms)[a]

	SimAWQ			SimCYH			SimRMH		
CypA−substrate interaction	trans	TS	cis	trans	TS	cis	trans	TS	cis
Phe113 $C_{\delta1}$−Pro*N* C_{γ}	3.94	3.90	3.71	5.58	3.76	3.92	4.32	3.75	4.17
Leu122 $C_{\delta1}$−Pro*N* C_{β}	3.72	4.00	3.76	5.48	4.17	4.24	4.47	3.66	3.94
His126 $C_{\epsilon1}$−Xaa*N*−1 C	4.63	3.94	3.84	6.55	4.05	3.55	4.84	4.12	3.64
Arg55 $N_{\eta1}$−Pro*N* O	2.82	2.79	2.81	4.57	3.67	6.79	2.94	2.85	2.82
Asn102 O−Xaa*N*−1 N	3.77	2.95	3.10	6.47	3.25	2.85	5.16	3.03	2.80

[a] Pro*N* and Xaa*N*−1 refer to the target proline and the residue preceding the target proline in the substrate, respectively. The letter following the residue label refers to the atom.

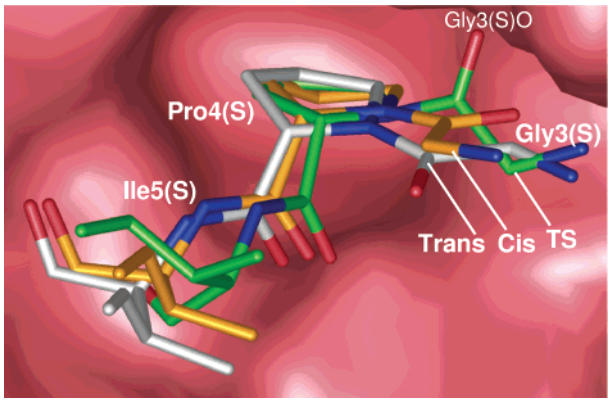

FIGURE 3: View of the CypA active site based on average structures from the trans, TS, and cis forms of SimAWQ. CypA is represented with a pink surface, and only residues 3−5 of the substrate peptide are shown. Pro4(S) is the target proline. The proline ring exhibits a small deviation, while Gly3(S) O rotates 180° between trans and cis structures. This figure was generated using PyMOL (*86*).

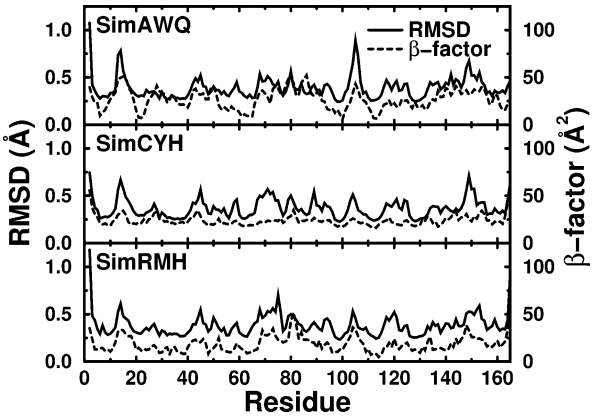

FIGURE 4: Dynamical flexibility of the human CypA backbone. The solid curve shows the computed rms deviations for C_{α} over a 2 ns MD run, and the dashed line represents the β-factor values (obtained from X-ray structures corresponding to the Sim types). For SimCYH and SimRMH, a trajectory with an ω of 0° was used, and for SimAWQ, an ω of 180° (representing structures similar to the X-ray crystal structure) was used.

preceding residue rotates 180°. Quantum-mechanical modeling of the active site based on trans and TS structures (data not shown) indicates single bond character for the peptide bond closer to the TS. This observation is based on inspection of localized molecular orbitals (see ref *81* for details of a similar analysis). Stronger interactions are present between the substrate peptide and CypA residues in the TS and cis state structures (Table 1). Several hydrophobic contacts between Pro*N*(S) and conserved CypA residues are considerably shorter in these states, indicating stabilization of the target proline ring. Hydrogen bonds from Pro*N*(S) O to the guanidino group of Arg55, and from Asn102 O to Xaa*N*−1(S) N[5] are stronger in the TS and cis average structures. Fluctuations in these crucial interactions during the course of reaction, especially close to the TS, would change the nature of the peptide bond. Such rearrangements have previously been observed in the active site of other enzymes based on quantum-mechanical modeling (*29*, *81*). For SimCYH, we observed strong interaction (2.46 Å) between Arg55 $N_{\eta2}$ and the carboxyl terminus of Pro*N*(S) at TS, which is consistent with the suggested reason for the Ala-Pro peptide acting as a competitive inhibitor of CypA (*51*).

Our observations are consistent with insights from recent structural and computational studies. Structural changes observed in this study support the reaction mechanism suggested by Howard et al. (*54*), which requires minimum deviation from the ground state crystal structure and displays single bond character for the peptide bond near the TS. Using a methodology similar to that in this paper, investigation of cis−trans isomerization in CA^N catalyzed by CypA has provided additional details about the reaction mechanism (*56*). The structural rearrangements in the active site observed in this study and ref *56* are also similar to those reported by Bruice and co-workers (*53*), and the strong interactions between the substrate and Arg55 agree with the calculations of Cui and co-workers (*55*).

Significant differences were found when the CypA reaction mechanism was compared with that of another PPIase, the FK506 binding protein (FKBP) (*47*), as also observed by Cui and co-workers (*55*).

Conformational Flexibility of the Backbone. The dynamical conformational flexibility of the CypA backbone was assessed by calculating rms deviations observed in the 2 ns MD run structures. Results indicate that the CypA backbone displays a high degree of flexibility in several regions: residues 12−18, 42−48, 64−78, 101−108, 118−126, and 146−154. These regions are in qualitative agreement with the temperature factors (β-factors) available from the X-ray structures (Figure 4). Computed rms deviations for the backbone N were also found to be in agreement with the NMR relaxation studies (*12*) in the following regions: residues 68−72, 82, and 97−103.

The movement of the CypA backbone in certain regions probably impacts the reaction. The flexible region of residues 101−104 is present in the active site, with residues Asn102 and Ala103 making close contacts with Pro*N*(S) and Xaa*N*−1(S). Changes in these interactions will alter the nature of

[5] Pro*N*(S) is the target proline of the substrate and Xaa*N*−1(S) is the residue preceding Pro*N*(S); the label after residue name refers to the atom in the residue.

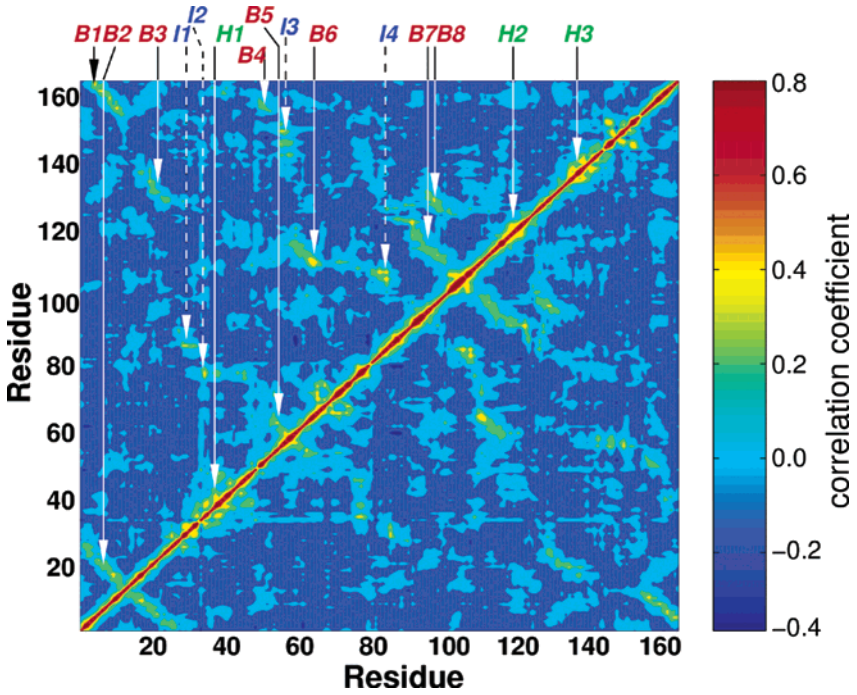

FIGURE 5: DCCM of human CypA computed for SimAWQ 2 ns MD runs at the TS (based on the center of mass of residues). Results from trans and cis forms, and other Sim types, are similar. The areas of significant correlation are labeled as follows: B1 for the correlation between β-strands S1 and S8, B2 for that between S1 and S2, B3 for that between S2 and S7, B4 for that between S3 and S8, B5 for that between S3 and S4, B6 for that between S4 and S6, B7 for that between S5 and S6, and B8 for that between S5 and S7. H1 is the correlation between residues of α-helix 1 (residues 30−41), H2 that between residues of α-helix 2 (residues 120−122), and H3 that between residues of α-helix 3 (residues 136−144). I1 is the correlation between residues 29−33 and 85 and 86, I2 that between residues 34−36 and 77 and 78, I3 that between residues 56 and 57 and 142−150, and I4 that between residues 82−85 and 104−108. The locations of β-strands are as follows: S1, residues 4−11; S2, 16−24; S3, 50−56; S4, 61−64; S5, 96−101; S6, 111−116; S7, 127−134; and S8, 155−164.

the peptide bond (see the previous sub-section). Dynamical fluctuation in this region will change the nature of these CypA−substrate interactions and therefore impact the reaction.

Correlated Motions of Residues. CypA regions displaying correlated motions were identified by examining the DCCM (Figure 5). Areas of largest correlation along the diagonal of DCCM (residues 30−41, 120−122, and 136−144) represent concerted motions of residues within α-helices. The majority of the off-diagonal areas exhibiting a high degree of correlation represent the concerted motions of β-strands (interactions between different β-strands are labeled in Figure 5; see the legend for more details). Some areas of the DCCM exhibiting significant correlation, however, are not associated with secondary structure elements. Residues 85 and 86 exhibit correlation with residues 29−33 (area I1 in Figure 5). Residues 77 and 78 display correlation with residues 34−36 (area I2). Residues 56 and 57 are correlated with residues 142−150 (area I3). Residues 82−85 are significantly correlated with residues 104−108 (area I4).

Individual residue pairs displaying highly correlated movements were also identified (Tables 2 and 3). Results indicate that more than 25 residue pairs exhibit highly correlated motions, with several pairs involving conserved[6] residues: Phe83 shows highly correlated motion with Asn108; motion of Glu86 is highly correlated to those of Val29, Pro30, Thr32, and Ala33; the side chain of Thr107 displays correlated motions with those of Asn102, Ala103, and Gly104; and motions of Gln111 and Gly72 are correlated.

Further structural analysis indicates that regions exhibiting highly correlated motions are connected through hydrogen bonds: residues 29−33 and 85 and 86, connected by hydrogen bonds between the side chain of Glu86 and Lys31/Thr32; residues 34−36 and 77 and 78, connected by the Asn35 $O_{\delta 1}$−Ile78 N hydrogen bond; loop residues 82 and 83 and 104−108 connected by the Phe83 N−Asn108 O hydrogen bond; and loop residues 56 and 57 and 142−150 connected by the Ile56 N−Gly150 O hydrogen bond. Note that Glu86, Thr32, and Asn35 are conserved residues and their side chains form these bridging hydrogen bonds.

Protein Vibrations. Protein vibrations closely coupled with the isomerization reaction were identified by quasi-harmonic analysis of system snapshots traversing the entire reaction path. The calculated eigenmodes represent the protein vibrational modes spanning the microsecond−millisecond time scale of the reaction. The analysis of the first 50 modes indicates that about 10 protein vibrational modes are associated with the rotation of the peptide bond. Illustrated in Figure 6 and described below are three modes associated with the largest peptide bond rotations (listed in decreasing order). Animation movies of these modes are available in the Supporting Information. The results presented here are from SimAWQ, but similar modes were found for SimCYH and SimRMH.

In mode A, significant displacements are present in residues 13−18, 58−60, 78−81, 117−125, and 136−152. Large atomic displacements are displayed by Pro*N*(S), Xaa*N*−1(S), CypA residues 102 and 103, and the side chain of conserved residue Phe60, which makes hydrophobic contacts with the Pro*N*(S) ring. Considerable fluctuations were observed in the lengths of hydrogen bonds from the

[6] See Figure 1 for genomic analysis for conserved residues.

Table 2: Significant Cross-Correlation Coefficients for the Center of Mass of Residue Pairs[a]

	SimAWQ			SimCYH			SimRMH			
residue pair	trans	TS	cis	trans	TS	cis	trans	TS	cis	$C_\alpha-C_\alpha$ distance (Å)
60−57	0.473	0.470	0.506	0.464	0.503	0.450	0.432	0.420	0.435	5.51
74−68	0.474	0.460	0.524	0.578	0.588	0.486	0.461	0.603	0.515	5.83
75−68	0.426	0.417	0.463	0.497	0.561	0.421	0.445	0.523	0.449	5.01
77−35	0.499	0.501	0.472	0.514	0.471	0.496	0.527	0.474	0.478	6.39
78−35	0.502	0.503	0.472	0.540	0.479	0.530	0.544	0.543	0.525	5.93
78−38	0.380	0.340	0.364	0.385	0.338	0.387	0.335	0.357	0.349	7.50
79−35	0.392	0.360	0.349	0.362	0.327	0.369	0.407	0.395	0.327	8.03
86−29	0.391	0.456	0.516	0.505	0.443	0.449	0.389	0.380	0.431	6.50
86−30	0.413	0.468	0.501	0.476	0.437	0.413	0.399	0.403	0.441	8.33
86−32	0.401	0.428	0.522	0.492	0.527	0.469	0.396	0.483	0.432	6.88
106−84	0.360	0.380	0.439	0.471	0.424	0.315	0.508	0.442	0.476	3.89
107−83	0.374	0.338	0.380	0.453	0.330	0.411	0.425	0.303	0.396	5.73
107−85	0.406	0.315	0.365	0.452	0.323	0.452	0.451	0.388	0.439	7.41
107−102	0.449	0.479	0.413	0.544	0.472	0.541	0.488	0.453	0.482	5.54
107−103	0.522	0.583	0.589	0.639	0.586	0.585	0.583	0.500	0.611	5.89
107−104	0.571	0.593	0.510	0.660	0.615	0.569	0.658	0.545	0.613	6.12
108−83	0.537	0.551	0.529	0.589	0.521	0.592	0.595	0.502	0.578	5.23
108−84	0.387	0.421	0.348	0.380	0.346	0.499	0.490	0.373	0.458	6.29
108−85	0.576	0.536	0.550	0.596	0.559	0.631	0.576	0.525	0.611	6.79
108−104	0.397	0.333	0.314	0.435	0.329	0.434	0.452	0.346	0.444	8.64
109−35	0.334	0.357	0.399	0.384	0.360	0.342	0.381	0.328	0.370	8.72
109−77	0.400	0.341	0.464	0.416	0.411	0.424	0.439	0.344	0.385	4.52
111−65	0.401	0.484	0.485	0.479	0.403	0.515	0.405	0.431	0.401	4.06
123−92	0.580	0.540	0.632	0.524	0.516	0.564	0.459	0.507	0.525	6.17
128−90	0.374	0.354	0.445	0.334	0.379	0.388	0.384	0.366	0.413	5.57
143−58	0.434	0.427	0.463	0.475	0.508	0.516	0.386	0.446	0.377	5.32
146−56	0.489	0.422	0.525	0.431	0.476	0.501	0.486	0.469	0.438	4.60
147−56	0.471	0.376	0.411	0.361	0.382	0.420	0.374	0.403	0.349	6.46
150−56	0.569	0.503	0.500	0.497	0.464	0.420	0.422	0.478	0.374	4.57
150−57	0.477	0.433	0.444	0.375	0.422	0.438	0.421	0.426	0.356	4.87

[a] The last column gives the distance between C_α atoms of the residue pair, averaged over three X-ray structures (PDB entries 1AWQ, 2CYH, and 1RMH). Neighboring residues ($|i - j| < 3$) and residue pairs involved in secondary structure formation are not listed.

guanidino group of Arg55 to Pro*N*(S) O, and from Asn102 O to Xaa*N*−1(S) N. The displacements indicated in this mode would affect both hydrophobic and hydrophilic CypA−substrate interactions, and therefore impact the isomerization of the peptide bond.

In mode B, large motions are present in residues 68−76, 80−83, 89−93, and 101−106, with additional motions in residues 12−15, 120−125, and 142−144. Residues 68−76, 80−83, and 89−93 are a part of a long surface loop region (residues 65−96); side chains of several residues of this loop region are exposed to the solvent and display large displacements. This loop is connected to another loop (residues 101−108) by hydrogen bonding between residues 83 and 108. Note that DCCM indicated that motions of these two loop regions are highly correlated. In this mode, the motions of residues 101−104 are found to be concerted with those of the substrate peptide; atoms of Ala103 are displaced toward the substrate peptide, which in turn rotates to avoid steric hindrance. The CypA−substrate hydrophobic interactions change considerably in this mode.

In mode C, the largest motions are present in residues 101−107 with additional motions in residues 120−125. These two regions are connected by a hydrogen bond between the side chain of Asn102 and the backbone of Lys125. The length of hydrogen bonds between Asn102 and Xaa*N*−1(S) and those between Arg55 and Pro*N*(S) vary in this mode, with the variations being large in the case of the former. The hydrophobic interactions between the Pro*N*(S) ring and Phe60 also vary in this mode.

Other protein vibrational modes associated with peptide bond rotation display similar (but smaller) motions. These motions are present in a combination of regions already described in modes A−C, and two additional regions (residues 24−33 and 69−71).

It is interesting to note that the regions displaying high activity in these vibrational modes have large temperature factors (see Figure 4). NMR relaxation studies have also detected motions in these regions only during substrate turnover (*12*). Further, several surface loop regions associated with large displacements of the CypA backbone are connected to internal regions through hydrogen bonds and hydrophobic interactions. These internal regions also exhibit large displacements and are either present in the active site or in the vicinity of the active site.

Effect of Protein Vibrations on the Reaction. The effects of protein vibrations on the energetics of the reaction (close to TS) were investigated by quantum-mechanical modeling of the CypA active site. Such calculations for the complete system with solvent are not possible in the current framework, because the protein vibrational modes were calculated for only solute atoms and no information about solvent movement in these vibrational modes is available. As an approximate analysis, we obtained energy surfaces for system displacement along the protein vibrational modes of interest by performing quantum-mechanical calculations on a small model of the active site. Similar quantum-mechanical calculations for enzyme active site models have been reported previously (*81*). The 192-atom model of the CypA active site used in this study, based on the TS of SimAWQ, consists of CypA residues 55, 60, 61, 102, 103, 113, 122, and 126 and residues 3−5 for the substrate peptide. Results indicate that when the system in the vicinity of TS is displaced along

Table 3: Significant Cross-Correlation Coefficients for Side Chain Atoms of Residue Pairs[a]

	SimAWQ			SimCYH			SimRMH			
residue pair	trans	TS	cis	trans	TS	cis	trans	TS	cis	$C_\alpha-C_\alpha$ distance (Å)
64−54	0.341	0.306	0.383	0.419	0.352	0.381	0.334	0.306	0.230	5.71
74−68	0.618	0.605	0.660	0.711	0.687	0.599	0.606	0.754	0.682	5.83
77−35	0.405	0.399	0.356	0.436	0.387	0.422	0.456	0.378	0.382	6.39
78−35	0.390	0.388	0.348	0.389	0.360	0.381	0.409	0.393	0.377	5.93
78−38	0.343	0.313	0.310	0.344	0.315	0.357	0.307	0.341	0.320	7.50
86−29	0.460	0.359	0.456	0.393	0.373	0.390	0.374	0.335	0.345	6.50
86−30	0.421	0.398	0.385	0.407	0.315	0.383	0.354	0.328	0.391	8.33
86−32	0.715	0.661	0.684	0.670	0.638	0.667	0.673	0.641	0.648	6.88
86−33	0.312	0.335	0.338	0.332	0.290	0.335	0.275	0.315	0.296	10.02
99−92	0.377	0.355	0.341	0.336	0.355	0.283	0.271	0.366	0.383	7.97
107−85	0.336	0.278	0.223	0.407	0.273	0.339	0.408	0.326	0.389	7.41
107−102	0.364	0.368	0.302	0.402	0.399	0.525	0.389	0.354	0.460	5.54
107−103	0.565	0.620	0.670	0.676	0.628	0.692	0.605	0.552	0.671	5.89
107−104	0.585	0.552	0.510	0.637	0.587	0.598	0.595	0.479	0.569	6.12
108−85	0.540	0.478	0.415	0.442	0.384	0.392	0.536	0.433	0.573	6.79
108−103	0.275	0.275	0.246	0.344	0.273	0.333	0.335	0.223	0.292	7.68
108−104	0.292	0.291	0.207	0.365	0.249	0.378	0.365	0.295	0.434	8.64
111−72	0.419	0.345	0.397	0.439	0.524	0.474	0.430	0.322	0.343	7.57
113−101	0.378	0.268	0.332	0.311	0.344	0.319	0.344	0.271	0.250	6.18
117−95	0.250	0.279	0.292	0.251	0.269	0.238	0.296	0.282	0.247	4.46
121−60	0.305	0.385	0.353	0.427	0.302	0.248	0.371	0.331	0.307	11.40
122−92	0.295	0.310	0.362	0.331	0.319	0.343	0.225	0.316	0.299	6.93
146−56	0.304	0.268	0.345	0.242	0.340	0.354	0.359	0.326	0.279	4.60
150−57	0.209	0.240	0.355	0.242	0.277	0.320	0.302	0.334	0.243	4.87
163−37	0.465	0.462	0.570	0.584	0.397	0.594	0.547	0.514	0.509	7.14

[a] The last column gives distances between C_α atoms of the residue pair, averaged over three X-ray structures (PDB entries 1AWQ, 2CYH, and 1RMH). Neighboring residues ($|i - j| < 3$) and residue pairs involved in secondary structure formation are not listed. For these calculations, the positions of the following last side chain heavy atoms were used: C_α for Gly, C_β for Ala, $C_{\gamma1}$ for Val, $C_{\delta1}$ for Leu and Ile, C_ϵ for Met, C_γ for Pro, C_ζ for Phe, $C_{\eta2}$ for Trp, O_γ for Ser, $O_{\gamma1}$ for Thr, $O_{\delta1}$ for Asp and Asn, $O_{\epsilon1}$ for Glu and Gln, O_η for Tyr, S_γ for Cys, N_ζ for Lys, $N_{\eta1}$ for Arg, and $C_{\epsilon1}$ for His.

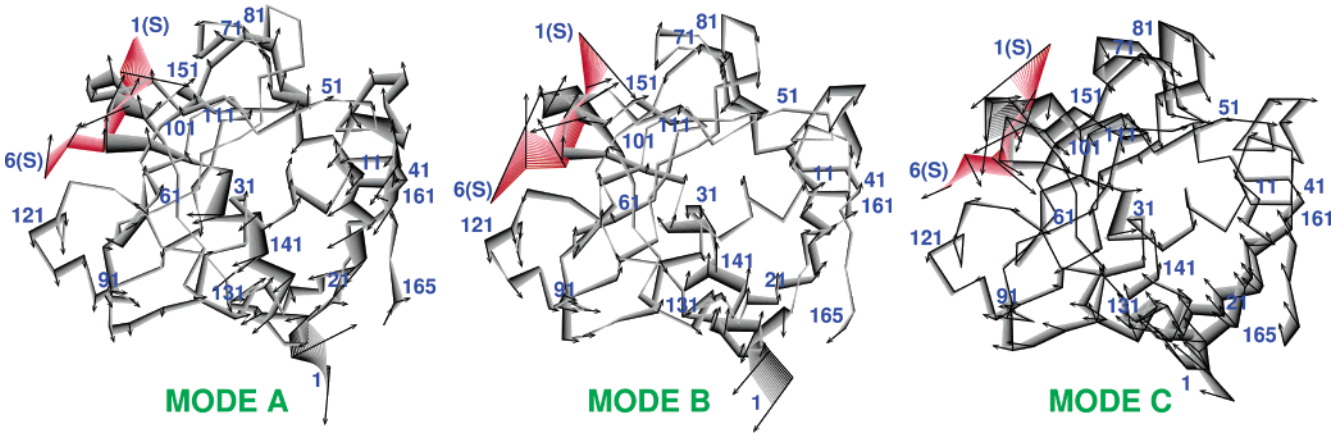

FIGURE 6: Illustration of protein vibrational modes associated with the peptide bond isomerization catalyzed by human CypA. Modes A−C from SimAWQ are shown (see the text for more details). Motions (only for C_α atoms) are shown in a movie-like fashion with lighter shades representing subsequent frames in the movie. The substrate peptide is in red and CypA in black. Dark arrows represent the displacement vectors for C_α atoms, and numbers correspond to C_α atoms.

protein vibrational modes, the product side is energetically more favorable than the reactant side (Figure 7). These early indications, therefore, suggest that these vibrational modes probably aid in promoting catalysis. Note that this model does not have the complete enzyme or the solvent, so a direct energy comparison between this figure and free energy profiles is not very meaningful. Further, the complete energy change along the reaction path will be a sum of contributions of all protein vibrational modes and not just modes A−C. To reiterate, our preliminary calculations demonstrate that certain protein vibrational modes (thermodynamical fluctuations) coupled to the reaction have energetic consequences in the regions close to the TS, and therefore are a contributing factor in the determination of the free energy barrier height. A detailed analysis of such calculations could be the subject of future investigations.

Motion of Residues over the Course of the Reaction. Examination of key interactions over the course of the reaction provides further insights about protein vibrations (Figures 8 and 9). Several distances in the active site and distal to the active site were monitored on the basis of results of correlation studies and quasi-harmonic analysis. For these distance profiles, the reaction coordinate ($\Delta\omega$) is described as a change in ω relative to the trans form. These profiles provide information about the microsecond−millisecond time scale of the reaction. The fluctuations exhibited in these

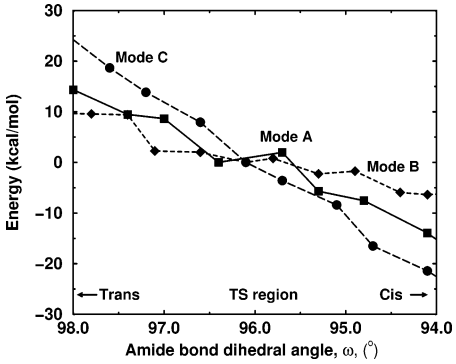

FIGURE 7: Energy profiles from quantum-mechanical ab initio calculations for the CypA active site model displaced along protein vibrational modes A−C.

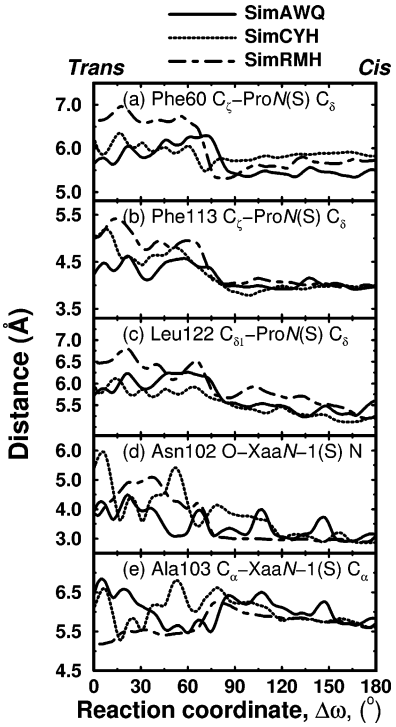

FIGURE 8: Variation of key active site interactions along the reaction profile. The reaction coordinate, $\Delta\omega$, is the change in the amide bond dihedral angle relative to the trans form: (a) Phe60 C_ζ−Pro*N*(S) C_δ, (b) Phe113 C_ζ−Pro*N*(S) C_δ, (c) Leu122 $C_{\delta1}$−Pro*N*(S)-C_δ, (d) Asn102 O−Xaa*N*−1(S) N, and (e) Ala103 C_α−Xaa*N*−1(S) C_α.

distances profiles occur along the entire reaction path, indicating that the displacements observed in protein vibrational modes are present on the time scale of the reaction.

Interactions around the target proline display fluctuations along the reaction profile (Figure 8). Dynamical fluctuations are observed in hydrophobic interactions of conserved residues Phe60, Phe113, and Leu122 with the Pro*N*(S) ring. In addition to the fluctuations, these interactions change considerably close to the TS. The distance between Ala103 and Xaa*N*−1(S) also displays dynamic variation along the reaction profile. Key hydrophilic interactions in the active site also exhibit similar behavior; the distance between Asn102 O and Xaa*N*−1(S) N exhibits an oscillatory pattern along the reaction profile. As indicated by structural analysis, these CypA−substrate interactions are fairly strong close to the TS, and dynamical fluctuations in the active site will influence the reaction.

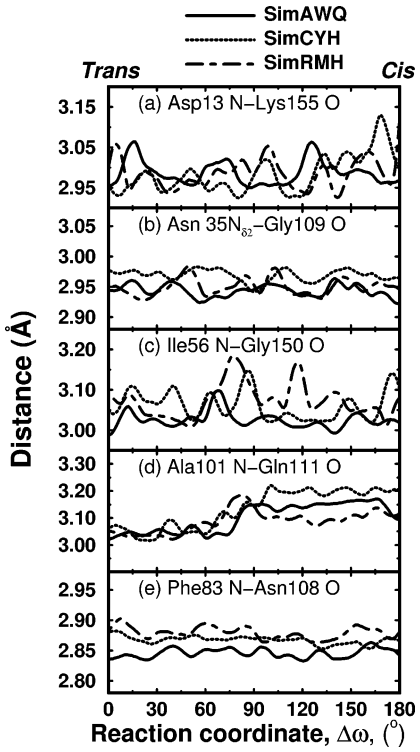

FIGURE 9: Variation of important interactions (distal to active site) along the reaction profile. The reaction coordinate, $\Delta\omega$, is the change in the amide bond dihedral angle relative to the trans form: (a) Asp13 N−Lys155 O, (b) Asn35 $N_{\delta2}$−Gly109 O, (c) Ile56 N−Gly150 O, (d) Ala101 N−Gln111 O, and (e) Phe83 N−Asn108 O.

Like the active site interactions, several interactions within CypA also display fluctuations along the reaction profile (Figure 9), even though they are located several angstroms from the active site. We monitored several hydrogen bonds connecting high-mobility regions. The Asp13 N−Lys155 O bond (located more than 20 Å from C_α of the target proline) connects the loops of residues 12−15 and 146−155. The Asn35 $N_{\delta2}$−Gly109 O bond (>14 Å away) connects the α-helix with a loop close to active site β-strand S6.[7] The Ile56 N−Gly150 O bond (>10 Å away) connects active site β-strand S3 with the loop of residues 146−155. The Ala101 N−Gln111 O bond (>7 Å away) connects active site β-strands S5 and S6. The Phe83 N−Asn108 O bond (>14 Å away) connects loops of residues 76−86 and 101−108. Note that Ile56 N−Gly150 O and Ala101 N−Gln111 O bonds exhibit additional activity close to the TS. Other randomly selected interactions did not show these fluctuations. Small differences between Sim types in these profiles may be due to the presence of different peptide substrates.

Similar fluctuations in these distance profiles have also been observed for the CypA-catalyzed isomerization in CA^N from HIV-1 (*56*).

Network of Protein Vibrations. We propose that high-mobility regions of CypA and the contacts between them form a network of protein vibrations coupled to the reaction, extending from the surface to the active site residues (Figure 10). On the basis of the conformational flexibility of the CypA backbone, correlation between residues and vibrational modes, three parts of this network can be formulated.

[7] For β-strand sequences, see the legend of Figure 5.

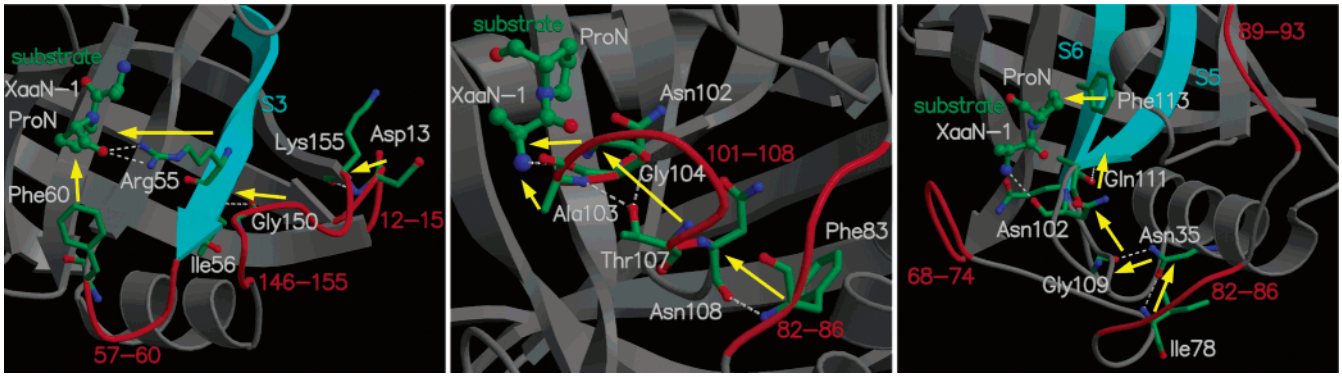

FIGURE 10: Diagram of the network of protein vibrations. Yellow arrows represent the network pathway. Flexible surface loops are denoted and numbered in red. Only two residues of the substrate peptide are shown, but the network can be applied to larger substrates, as well. This figure was generated with MOLSCRIPT and RASTER3D (*87*, *88*).

Table 4: Conservation of Network Hydrogen Bonds in Cyclophilin Structures from Various Species[a]

human CypA (1AWQ/2CYH/1RMH average)	Asp13 N−Lys155 O	Asn35 $N_{\delta2}$−Gly109 O	Ile56 N−Gly150 O	Ala101 N−Gln111 O	Phe83 N−Asn108 O
	2.89	3.01	2.96	3.04	2.87
human cyclophilin B (1CYN)	Gly21 N−Asp164 O	Asn43 $N_{\delta2}$−Gly117 O	Val64 N−Asp159 O	Ala109 N−Gln119 O	Phe91 N−Asn116 O
	2.91	3.06	3.00	3.05	2.75
Brugia malayi (1A33)	Asp16 N−Asp167 O	Asn38 $N_{\delta2}$−Gly120 O	Val67 N−Asn162 O	Ala112 N−Gln122 O	Phe94 N−Asn119 O
	2.89	2.92	3.05	3.06	2.85
C. elegans cyclophilin 3 (1DYW)	Gly13 N−Asp162 O	Asn35 $N_{\delta2}$−Gly116 O	Ile63 N−Gly157 O	Ala108 N−Gln118 O	Phe90 N−Asn115 O
	2.85	3.09	2.96	2.98	2.94
C. elegans cyclophilin 5 (1H0P)	Gly37 N−Asp180 O	Asn59 $N_{\delta2}$−Gly133 O	Val80 N−Asp175 O	Ala125 N−Gln135 O	Phe107 N−Asn132 O
	2.78	2.91	2.85	3.09	2.93
B. taurus PPIase (1IHG)	Gly25 N−Leu175 O	Asn47 $N_{\delta2}$−Gly129 O	Ile76 N−Glu170 O	Ala121 N−Gln131 O	Phe103 N−Asn128 O
	2.98	3.21	2.84	3.07	2.84
Plasmodium falciparum cyclophilin (1QNG)	Asp14 N−Ser162 O	Asn36 $N_{\delta2}$−Ser116 O	Ile63 N−Gly157 O	Ala108 N−Gln118 O	Phe90 N−Asn115 O
	2.74	2.88	2.93	3.05	2.80
E. coli PPIase (2NUL)	Asn7 N−Ile156 O	Asn26 $N_{\delta2}$−Thr95 O	Val44 N−Asp149 O	Ala86 N−Gln97 O	Ile68 N−Ala94 O
	2.90	2.67	2.97	2.88	2.76

[a] Three-dimensional structures were aligned using secondary structure elements, and equivalent hydrogen bonds were selected on the basis of sequence and structural similarities. Hydrogen bond lengths are in given angstroms, and PDB codes are given in parentheses.

(1) Highly flexible loops 12−15 and 146−155 are connected by the Asp13 N−Lys155 O hydrogen bond. The loop region 146−155 in turn is linked to β-strand S3 by the Ile56 N−Gly150 O hydrogen bond. β-Strand S3 lines the active site and contains the catalytically important Arg55. The guanidino group of Arg55 forms critical hydrophilic contacts with Pro*N*(S) O. Another flexible loop (residues 57−60) connects β-strands S3 and S4. Conserved residue Phe60 located on this loop interacts with the Pro*N*(S) ring.

(2) Highly flexible surface loop regions 66−95 and 101−108 are connected by a strong Phe83 N−Asn108 O hydrogen bond. Side chain atoms of the conserved Thr107 residue form hydrogen bonds with the backbone of Ala103 and Gly104. Ala103, an active site residue, forms hydrophobic interactions with the substrate peptide. Neighboring residue Asn102 forms important hydrophilic contacts with Xaa*N*−1(S).

(3) The flexible surface loop region 68−74 forms a link to Gly109 via two hydrogen bonds (Asn35 $O_{\delta1}$−Ile78 N and Asn35 $N_{\delta2}$−Gly109 O). In addition, Asn35 is a part of an α-helix and its neighboring residues (29−33) form additional contacts with the surface region of residues 82−86. Gly109 is located close to active site β-strand S6. S6 contains Phe113, which makes important hydrophobic contacts with the Pro*N*(S) ring. Further, Gln111 from S6 is connected to S5 by the Ala101 N−Gln111 O hydrogen bond. Residues Asn102 and Ala103 of S5 form crucial hydrophobic and hydrophilic contacts with the peptide.

Vibrations in these network parts impacts catalysis by altering crucial interactions between the CypA residues and peptide substrate. A somewhat similar network of coupled motions has been identified previously for hydride transfer in dihydrofolate reductase (*29*). That network, however, was characterized on the basis of thermally averaged changes over the course of reaction. In contrast, this dynamical network of vibrations in CypA influences states all along the course of the reaction. We state that parts of the network described above are most likely not complete or unique. Further, this study cannot differentiate between motions influencing catalysis or motions arising as a result of alterations caused by catalysis. Collaborative experimental and theoretical studies could resolve this issue.

Evidence for the existence of this network comes from conservation of its parts in several species and observed protein motions during experimental studies. Table 4 shows

the conservation of five network hydrogen bonds in 10 cyclophilin structures from six different species. NMR relaxation studies have detected motions in Arg55, Lys82, Ala101, Asn102, Ala103, and Gly109 during only substrate turnover. All these residues form crucial points in the network. In addition, several network residues have large temperature factors possibly indicating vibrations.

DISCUSSION

This paper presents a theoretical approach to investigating the link between protein dynamics and enzymatic catalysis. A variety of computational techniques were utilized to study structural changes and motions in the enzyme−substrate complex, at multiple time scales, during the cis−trans isomerization catalyzed by human cyclophilin A. The results have identified a network of protein vibrations coupled to the reaction, extending from the surface of the enzyme to the active site. The vibrations in this network range from picosecond to microsecond−millisecond time scales. Indications are that the network impacts catalysis by affecting the interactions between CypA residues and the substrate.

The presence of this network has recently been confirmed for a naturally occurring and biologically relevant substrate for CypA (*56*). Investigations of cis−trans isomerization catalyzed by CypA in the 146-amino acid N-terminal domain of the HIV-1 capsid protein have shown results similar to those presented here. Further, to rule out any artifacts arising from use of the AMBER parm98 force field, we performed additional simulations for AWQ using the point-charge force field recently developed by Duan et al. (*82*) and the GROMOS96 43a1 force field (*83*). The force field from Duan et al. is based on condensed phase quantum-mechanical calculations and corrects for helical bias observed for proteins in previous force fields. The free energy profile, DCCM from the TS, and protein vibrational modes from SimAWQ and new simulations are compared in the Supporting Information. The results from parm98, Duan et al., and GROMOS96 43a1 force fields are very similar with almost no differences. This agreement rules out any artifacts from force fields and provides additional validation of the observations and results presented in this paper.

This type of network could provide new insights into enzymatic catalysis as well as allostericity and has broad implications for protein engineering and drug design. The identified vibrations may act as channels of energetic connectivity over long ranges in protein structure; genetic and mutational studies of the PDZ domain family have presented evidence for the existence of such channels (*84*). Energy exchange between these coupled vibrational modes as suggested by MD simulation of myoglobin is quite probable (*85*). Additionally, the observed correlation between various secondary structure elements and loop regions provides some insights into understanding allostericity. Changes can possibly be transmitted through a series of dynamical interactions between distal regions of the protein. Local conformational interactions between adjacent β-strands, occurring on the microsecond to millisecond time scales, have been reported for ribonuclease A (*11*).

Insights into protein dynamics, together with the knowledge of enzyme structure, could enhance our understanding of enzyme function. This presents interesting opportunities; biochemical studies can be designed to interrupt protein vibrations and dynamical interactions, either by breaking interactions between structural elements or by damping the vibrations with heavier residues. Such investigations could provide further insights into enzymatic catalysis, allosteric effects, and cooperative effects.

ACKNOWLEDGMENT

We thank Drs. Simon P. Webb, Bryan C. Hathorn, Dean A. Myles, and Jeffrey A. Nichols for stimulating discussions and Dr. Brahma Ghosh for feedback on the manuscript.

SUPPORTING INFORMATION AVAILABLE

Animation movies of protein vibrational modes A−C from SimAWQ (MPEG) and results from simulations with Duan et al. and GROMOS96 43a1 force fields. This material is available free of charge via the Internet at http://pubs.acs.org.

REFERENCES

1. Hammes, G. G. (2002) Multiple conformational changes in enzyme catalysis, *Biochemistry 41*, 8221−8228.
2. Wand, A. J. (2001) Dynamic activation of protein function: A view emerging from NMR spectroscopy, *Nat. Struct. Biol. 8*, 926−931.
3. Benkovic, S. J., and Hammes-Schiffer, S. (2003) A perspective on enzyme catalysis, *Science 301*, 1196−1202.
4. Falzone, C. J., Wright, P. E., and Benkovic, S. J. (1994) Dynamics of a flexible loop in dihydrofolate reductase from *Escherichia coli* and its implication for catalysis, *Biochemistry 33*, 439−442.
5. Epstein, D. M., Benkovic, S. J., and Wright, P. E. (1995) Dynamics of the dihydrofolate reductase-folate complex: Catalytic sites and regions known to undergo conformational change exhibit diverse dynamical features, *Biochemistry 34*, 11037−11048.
6. Cameron, C. E., and Benkovic, S. J. (1997) Evidence for a functional role of the dynamics of glycine-121 of *Escherichia coli* dihydrofolate reductase obtained from kinetic analysis of a site-directed mutant, *Biochemistry 36*, 15792−15800.
7. Kohen, A., Cannio, R., Bartolucci, S., and Klinman, J. P. (1999) Enzyme dynamics and hydrogen tunnelling in a thermophilic alcohol dehydrogenase, *Nature 399*, 496−499.
8. Kohen, A., and Klinman, J. P. (2000) Protein flexibility correlates with degree of hydrogen tunneling in thermophilic and mesophilic alcohol dehydrogenases, *J. Am. Chem. Soc. 122*, 10738−10739.
9. Osborne, M. J., Schnell, J., Benkovic, S. J., Dyson, H. J., and Wright, P. E. (2001) Backbone dynamics in dihydrofolate reductase complexes: Role of loop flexibility in the catalytic mechanism, *Biochemistry 40*, 9846−9859.
10. Bosco, D. A., Eisenmesser, E. Z., Pochapsky, S., Sundquist, W. I., and Kern, D. (2002) Catalysis of cis/trans isomerization in native HIV-1 capsid by human cyclophilin A, *Proc. Natl. Acad. Sci. U.S.A. 99*, 5247−5252.
11. Cole, R., and Loria, J. P. (2002) Evidence for flexibility in the function of ribonuclease A, *Biochemistry 41*, 6072−6081.
12. Eisenmesser, E. Z., Bosco, D. A., Akke, M., and Kern, D. (2002) Enzyme dynamics during catalysis, *Science 295*, 1520−1523.
13. Rajagopalan, P. T. R., and Benkovic, S. J. (2002) Preorganization and protein dynamics in enzyme catalysis, *Chem. Rec. 2*, 24−36.
14. Bu, Z. M., Neumann, D. A., Lee, S. H., Brown, C. M., Engelman, D. M., and Han, C. C. (2000) A view of dynamics changes in the molten globule-native folding step by quasielastic neutron scattering, *J. Mol. Biol. 301*, 525−536.
15. Tehei, M., Madern, D., Pfister, C., and Zaccai, G. (2001) Fast dynamics of halophilic malate dehydrogenase and BSA measured by neutron scattering under various solvent conditions influencing protein stability, *Proc. Natl. Acad. Sci. U.S.A. 98*, 14356−14361.
16. Gabel, F., Bicout, D., Lehnert, U., Tehei, M., Weik, M., and Zaccai, G. (2002) Protein dynamics studied by neutron scattering, *Q. Rev. Biophys. 35*, 327−367.
17. Lee, A. L., Sharp, K. A., Kranz, J. K., Song, X. J., and Wand, A. J. (2002) Temperature dependence of the internal dynamics of a calmodulin-peptide complex, *Biochemistry 41*, 13814−13825.

18. Williams, J. C., and McDermott, A. E. (1995) Dynamics of the flexible loop of triosephosphate isomerase: The loop motion is not ligand-gated, *Biochemistry 34*, 8309−8319.
19. Hernandez, G., Jenney, F. E., Adams, M. W. W., and LeMaster, D. M. (2000) Millisecond time scale conformational flexibility in a hyperthermophile protein at ambient temperature, *Proc. Natl. Acad. Sci. U.S.A. 97*, 3166−3170.
20. Zavodszky, P., Kardos, J., Svingor, A., and Petsko, G. A. (1998) Adjustment of conformational flexibility is a key event in the thermal adaptation of proteins, *Proc. Natl. Acad. Sci. U.S.A. 95*, 7406−7411.
21. Lolis, E., and Petsko, G. A. (1990) Crystallographic analysis of the complex between triosephosphate isomerase and 2-phosphoglycolate at 2.5-Å resolution: Implications for catalysis, *Biochemistry 29*, 6619−6625.
22. Lolis, E., Alber, T., Davenport, R. C., Rose, D., Hartman, F. C., and Petsko, G. A. (1990) Structure of yeast triosephosphate isomerase at 1.9-Å resolution, *Biochemistry 29*, 6609−6618.
23. Sawaya, M. R., and Kraut, J. (1997) Loop and subdomain movements in the mechanism of *Escherichia coli* dihydrofolate reductase: Crystallographic evidence, *Biochemistry 36*, 586−603.
24. Rader, S. D., and Agard, D. A. (1997) Conformational substates in enzyme mechanism: The 120 K structure of α-lytic protease at 1.5 Å resolution, *Protein Sci. 6*, 1375−1386.
25. Radkiewicz, J. L., and Brooks, C. L. (2000) Protein dynamics in enzymatic catalysis: Exploration of dihydrofolate reductase, *J. Am. Chem. Soc. 122*, 225−231.
26. Rod, T. H., Radkiewicz, J. L., and Brooks, C. L., III (2003) Correlated motion and the effect of distal mutations in dihydrofolate reductase, *Proc. Natl. Acad. Sci. U.S.A. 100*, 6980−6985.
27. Antoniou, D., and Schwartz, S. D. (2001) Internal enzyme motions as a source of catalytic activity: Rate-promoting vibrations and hydrogen tunneling, *J. Phys. Chem. B 105*, 5553−5558.
28. Caratzoulas, S., Mincer, J. S., and Schwartz, S. D. (2002) Identification of a protein-promoting vibration in the reaction catalyzed by horse liver alcohol dehydrogenase, *J. Am. Chem. Soc. 124*, 3270−3276.
29. Agarwal, P. K., Billeter, S. R., Rajagopalan, P. T. R., Benkovic, S. J., and Hammes-Schiffer, S. (2002) Network of coupled promoting motions in enzyme catalysis, *Proc. Natl. Acad. Sci. U.S.A. 99*, 2794−2799.
30. Agarwal, P. K., Billeter, S. R., and Hammes-Schiffer, S. (2002) Nuclear quantum effects and enzyme dynamics in dihydrofolate reductase catalysis, *J. Phys. Chem. B 106*, 3283−3293.
31. Garcia-Viloca, M., Truhlar, D. G., and Gao, J. L. (2003) Reaction-path energetics and kinetics of the hydride transfer reaction catalyzed by dihydrofolate reductase, *Biochemistry 42*, 13558−13575.
32. Billeter, S. R., Webb, S. P., Agarwal, P. K., Iordanov, T., and Hammes-Schiffer, S. (2001) Hydride transfer in liver alcohol dehydrogenase: Quantum dynamics, kinetic isotope effects, and role of enzyme motion, *J. Am. Chem. Soc. 123*, 11262−11272.
33. Villa, J., and Warshel, A. (2001) Energetics and dynamics of enzymatic reactions, *J. Phys. Chem. B 105*, 7887−7907.
34. Hammes-Schiffer, S. (2002) Impact of enzyme motion on activity, *Biochemistry 41*, 13335−13343.
35. Cui, Q., and Karplus, M. (2003) Catalysis and specificity in enzymes: A study of triosephosphate isomerase and comparison with methyl glyoxal synthase, *Adv. Protein Chem. 66*, 315−372.
36. Guo, H., Cui, Q., Lipscomb, W. N., and Karplus, M. (2003) Understanding the role of active-site residues in chorismate mutase catalysis from molecular dynamics simulations, *Angew. Chem., Int. Ed. 42*, 1508−1511.
37. Watney, J. B., Agarwal, P. K., and Hammes-Schiffer, S. (2003) Effect of mutation on enzyme motion in dihydrofolate reductase, *J. Am. Chem. Soc. 125*, 3745−3750.
38. Gothel, S. F., and Marahiel, M. A. (1999) Peptidyl-prolyl cis−trans isomerases, a superfamily of ubiquitous folding catalysts, *Cell. Mol. Life Sci. 55*, 423−436.
39. Rovira, P., Mascarell, L., and Truffa-Bachi, P. (2000) The impact of immunosuppressive drugs on the analysis of T cell activation, *Curr. Med. Chem. 7*, 673−692.
40. Handschumacher, R. E., Harding, M. W., Rice, J., and Drugge, R. J. (1984) Cyclophilin: A specific cytosolic binding-protein for cyclosporin A, *Science 226*, 544−547.
41. Takahashi, N., Hayano, T., and Suzuki, M. (1989) Peptidyl-prolyl cis−trans isomerase is the cyclosporin A-binding protein cyclophilin, *Nature 337*, 473−475.
42. Fischer, G., Wittmannliebold, B., Lang, K., Kiefhaber, T., and Schmid, F. X. (1989) Cyclophilin and peptidyl-prolyl cis−trans isomerase are probably identical proteins, *Nature 337*, 476−478.
43. Fischer, G. (2000) Chemical aspects of peptide bond isomerisation, *Chem. Soc. Rev. 29*, 119−127.
44. Braaten, D., Franke, E. K., and Luban, J. (1996) Cyclophilin A is required for the replication of group M human immunodeficiency virus type 1 (HIV-1) and simian immunodeficiency virus SIV-(CPZ) GAB but not group O HIV-1 or other primate immunodeficiency viruses, *J. Virol. 70*, 4220−4227.
45. Wiegers, K., and Krausslich, H. G. (2002) Differential dependence of the infectivity of HIV-1 group O isolates on the cellular protein cyclophilin A, *Virology 294*, 289−295.
46. Gamble, T. R., Vajdos, F. F., Yoo, S. H., Worthylake, D. K., Houseweart, M., Sundquist, W. I., and Hill, C. P. (1996) Crystal structure of human cyclophilin A bound to the amino-terminal domain of HIV-1 capsid, *Cell 87*, 1285−1294.
47. Fischer, S., Michnick, S., and Karplus, M. (1993) A mechanism for rotamase catalysis by the FK506 binding protein (FKBP), *Biochemistry 32*, 13830−13837.
48. Van Duyne, G. D., Standaert, R. F., Karplus, P. A., Schreiber, S. L., and Clardy, J. (1993) Atomic structures of the human immunophilin FKBP-12 complexes with FK506 and rapamycin, *J. Mol. Biol. 229*, 105−124.
49. Galat, A., and Metcalfe, S. M. (1995) Peptidylproline cis/trans isomerases, *Prog. Biophys. Mol. Biol. 63*, 67−118.
50. Zhao, Y. D., and Ke, H. M. (1996) Crystal structure implies that cyclophilin predominantly catalyzes the trans to cis isomerization, *Biochemistry 35*, 7356−7361.
51. Zhao, Y. D., and Ke, H. M. (1996) Mechanistic implication of crystal structures of the cyclophilin-dipeptide complexes, *Biochemistry 35*, 7362−7368.
52. Ranganathan, R., Lu, K. P., Hunter, T., and Noel, J. P. (1997) Structural and functional analysis of the mitotic rotamase Pin1 suggests substrate recognition is phosphorylation dependent, *Cell 89*, 875−886.
53. Hur, S., and Bruice, T. C. (2002) The mechanism of cis−trans isomerization of prolyl peptides by cyclophilin, *J. Am. Chem. Soc. 124*, 7303−7313.
54. Howard, B. R., Vajdos, F. F., Li, S., Sundquist, W. I., and Hill, C. P. (2003) Structural insights into the catalytic mechanism of cyclophilin A, *Nat. Struct. Biol. 10*, 475−481.
55. Li, G., and Cui, Q. (2003) What is so special about Arg 55 in the catalysis of cyclophilin A? Insights from hybrid QM/MM simulations, *J. Am. Chem. Soc. 125*, 15028−15038.
56. Agarwal, P. K. (2004) Cis/trans isomerization in HIV-1 capsid protein catalyzed by cyclophilin A: Insights from computational and theoretical studies, *Proteins: Struct., Funct., Bioinf. 56*, 449−463.
57. Boeckmann, B., Bairoch, A., Apweiler, R., Blatter, M. C., Estreicher, A., Gasteiger, E., Martin, M. J., Michoud, K., O'Donovan, C., Phan, I., Pilbout, S., and Schneider, M. (2003) The SWISS-PROT protein knowledgebase and its supplement TrEMBL in 2003, *Nucleic Acids Res. 31*, 365−370.
58. Higgins, D. G., and Sharp, P. M. (1988) Clustal: A package for performing multiple sequence alignment on a microcomputer, *Gene 73*, 237−244.
59. Vajdos, F. E., Yoo, S. H., Houseweart, M., Sundquist, W. I., and Hill, C. P. (1997) Crystal structure of cyclophilin A complexed with a binding site peptide from the HIV-1 capsid protein, *Protein Sci. 6*, 2297−2307.
60. Pearlman, D. A., Case, D. A., Caldwell, J. W., Ross, W. S., Cheatham, T. E., Debolt, S., Ferguson, D., Seibel, G., and Kollman, P. (1995) AMBER, a package of computer programs for applying molecular mechanics, normal mode analysis, molecular dynamics and free energy calculations to simulate the structural and energetic properties of molecules, *Comput. Phys. Commun. 91*, 1−41.
61. Case, D. A., Pearlman, D. A., Caldwell, J. W., Cheatham, T. E., III, Wang, J., Ross, W. S., Simmerling, C. L., Darden, T. A., Merz, K. M., Stanton, R. V., Cheng, A. L., Vincent, J. J., Crowley, M., Tsui, V., Gohlke, H., Radmer, R. J., Duan, Y., Pitera, J., Massova, I., Seibel, G. L., Single, U. C., Weiner, P. K., and Kollman, P. (2002) *AMBER 7*, University of California, San Francisco.
62. Jorgensen, W. L., Chandrasekhar, J., Madura, J. D., Impey, R. W., and Klein, M. L. (1983) Comparison of simple potential functions for simulating liquid water, *J. Chem. Phys. 79*, 926−935.

63. Torrie, G. M., and Valleau, J. P. (1977) Nonphysical sampling distributions in Monte Carlo free-energy estimation: Umbrella sampling, *J. Comput. Phys. 23*, 187−199.
64. Northrup, S. H., Pear, M. R., Lee, C. Y., McCammon, J. A., and Karplus, M. (1982) Dynamical theory of activated processes in globular proteins, *Proc. Natl. Acad. Sci. U.S.A. 79*, 4035−4039.
65. Kumar, S., Bouzida, D., Swendsen, R. H., Kollman, P. A., and Rosenberg, J. M. (1992) The weighted histogram analysis method for free-energy calculations on biomolecules. 1. The method, *J. Comput. Chem. 13*, 1011−1021.
66. Boczko, E. M., and Brooks, C. L. (1993) Constant temperature free energy surfaces for physical and chemical processes, *J. Phys. Chem. 97*, 4509−4513.
67. Brooks, C. L., and Nilsson, L. (1993) Promotion of helix formation in peptides dissolved in alcohol and water-alcohol mixtures, *J. Am. Chem. Soc. 115*, 11034−11035.
68. Baudry, J., Crouzy, S., Roux, B., and Smith, J. C. (1999) Simulation analysis of the retinal conformational equilibrium in dark-adapted bacteriorhodopsin, *Biophys. J. 76*, 1909−1917.
69. Levitt, M., Sander, C., and Stern, P. S. (1985) Protein normal-mode dynamics: Trypsin inhibitor, crambin, ribonuclease and lysozyme, *J. Mol. Biol. 181*, 423−447.
70. Harte, W. E., Swaminathan, S., Mansuri, M. M., Martin, J. C., Rosenberg, I. E., and Beveridge, D. L. (1990) Domain communication in the dynamic structure of human immunodeficiency virus-1 protease, *Proc. Natl. Acad. Sci. U.S.A. 87*, 8864−8868.
71. Swaminathan, S., Harte, W. E., and Beveridge, D. L. (1991) Investigation of domain structure in proteins via molecular dynamics simulation: Application to HIV-1 protease dimer, *J. Am. Chem. Soc. 113*, 2717−2721.
72. Levy, R. M., Karplus, M., Kushick, J., and Perahia, D. (1984) Evaluation of the configurational entropy for proteins: Application to molecular dynamics simulations of an α-helix, *Macromolecules 17*, 1370−1374.
73. Teeter, M. M., and Case, D. A. (1990) Harmonic and quasiharmonic descriptions of crambin, *J. Phys. Chem. 94*, 8091−8097.
74. Frisch, M. J., Trucks, G. W., Schlegel, H. B., Scuseria, G. E., Robb, M. A., Cheeseman, J. R., Zakrzewski, V. G., Montgomery, J. A., Jr., Stratmann, R. E., Burant, J. C., Dapprich, S., Millam, J. M., Daniels, A. D., Kudin, K. N., Strain, M. C., Farkas, O., Tomasi, J., Barone, V., Cossi, M., Cammi, R., Mennucci, B., Pomelli, C., Adamo, C., Clifford, S., Ochterski, J., Petersson, G. A., Ayala, P. Y., Cui, Q., Morokuma, K., Malick, D. K., Rabuck, A. D., Raghavachari, K., Foresman, J. B., Cioslowski, J., Ortiz, J. V., Stefanov, B. B., Liu, G., Liashenko, A., Piskorz, P., Komaromi, I., Gomperts, R., Martin, R. L., Fox, D. J., Keith, T., Al-Laham, M. A., Peng, C. Y., Nanayakkara, A., Gonzalez, C., Challacombe, M., Gill, P. M. W., Johnson, B., Chen, W., Wong, M. W., Andres, J. L., Gonzalez, C., Head-Gordon, M., Replogle, E. S., and Pople, J. A. (1998) *Gaussian 98*, Gaussian Inc., Pittsburgh, PA.
75. Albers, M. W., Walsh, C. T., and Schreiber, S. L. (1990) Substrate specificity for the human rotamase FKBP: A view of FK506 and rapamycin as leucine (twisted amide) proline mimics, *J. Org. Chem. 55*, 4984−4986.
76. Harrison, R. K., and Stein, R. L. (1990) Substrate specificities of the peptidyl prolyl cis−trans isomerase activities of cyclophilin and FK-506 binding protein: Evidence for the existence of a family of distinct enzymes, *Biochemistry 29*, 3813−3816.
77. Kofron, J. L., Kuzmic, P., Kishore, V., Colonbonilla, E., and Rich, D. H. (1991) Determination of kinetic constants for peptidyl prolyl cis−trans isomerases by an improved spectrophotometric assay, *Biochemistry 30*, 6127−6134.
78. Kern, D., Kern, G., Scherer, G., Fischer, G., and Drakenberg, T. (1995) Kinetic-analysis of cyclophilin catalyzed prolyl cis/trans isomerization by dynamic NMR spectroscopy, *Biochemistry 34*, 13594−13602.
79. Truhlar, D. G., Gao, J. L., Alhambra, C., Garcia-Viloca, M., Corchado, J., Sanchez, M. L., and Villa, J. (2002) The incorporation of quantum effects in enzyme kinetics modeling, *Acc. Chem. Res. 35*, 341−349.
80. Garcia-Viloca, M., Alhambra, C., Truhlar, D. G., and Gao, J. (2001) Inclusion of quantum-mechanical vibrational energy in reactive potentials of mean force, *J. Chem. Phys. 114*, 9953−9958.
81. Webb, S. P., Agarwal, P. K., and Hammes-Schiffer, S. (2000) Combining electronic structure methods with the calculation of hydrogen vibrational wavefunctions: Application to hydride transfer in liver alcohol dehydrogenase, *J. Phys. Chem. B 104*, 8884−8894.
82. Duan, Y., Wu, C., Chowdhury, S., Lee, M. C., Xiong, G. M., Zhang, W., Yang, R., Cieplak, P., Luo, R., Lee, T., Caldwell, J., Wang, J. M., and Kollman, P. (2003) A point-charge force field for molecular mechanics simulations of proteins based on condensed-phase quantum mechanical calculations, *J. Comput. Chem. 24*, 1999−2012.
83. Scott, W. R. P., Hunenberger, P. H., Tironi, I. G., Mark, A. E., Billeter, S. R., Fennen, J., Torda, A. E., Huber, T., Kruger, P., and van Gunsteren, W. F. (1999) The GROMOS biomolecular simulation program package, *J. Phys. Chem. A 103*, 3596−3607.
84. Lockless, S. W., and Ranganathan, R. (1999) Evolutionarily conserved pathways of energetic connectivity in protein families, *Science 286*, 295−299.
85. Moritsugu, K., Miyashita, O., and Kidera, A. (2000) Vibrational energy transfer in a protein molecule, *Phys. Rev. Lett. 85*, 3970−3973.
86. DeLano Scientific (2002) *PyMOL*.
87. Kraulis, P. J. (1991) Molscript: A program to produce both detailed and schematic plots of protein structures, *J. Appl. Crystallogr. 24*, 946−950.
88. Merritt, E. A., and Bacon, D. J. (1997) Raster3D: Photorealistic molecular graphics, *Methods Enzymol. 277*, 505−524.

BI0495228